

Photocatalytic Water Splitting Using Oxynitride and Nitride Semiconductor Powders for Production of Solar Hydrogen

by Jun Kubota and Kazunari Domen

Water splitting using a photocatalyst for direct solar hydrogen production from sunlight and water, has been regarded as an important approach to artificial photosynthesis.^{1,2} Solar hydrogen, which is the simplest solar fuel, can then be converted to various energy carriers such as organic hydrides, methanol, methane, and ammonia for transportation and storage. Thus, energy systems based on solar hydrogen can lead to a stable, secure, and ecologically-friendly society. Although solar fuel production using electricity from photovoltaic cells and concentrated solar thermal power is an existing technology, direct synthesis of solar fuels by artificial photosynthesis has more scalability in terms of system cost.

To split water into hydrogen and oxygen, 1.23 V of energy is required, corresponding to a 2 electron reaction. An energy of 1.23 V is equivalent to a photon energy of 1000 nm, so that the visible light (400-800 nm in wavelength) that represents half of the solar energy spectrum can be thermodynamically used for water splitting. The challenge is to obtain an efficient photocatalyst that has an absorption edge in longer wavelength and the ability to split water.

Highly efficient oxide photocatalysts, such as La-doped NaTaO₃, and Zn-doped Ga₂O₃, have been reported with quantum efficiencies of over 50%.³⁻⁵ However, these oxides only absorb ultraviolet (UV) light with wavelengths shorter than 300 nm. In the solar spectrum at the earth's surface, such short UV light is not present, so that these oxides cannot operate efficiently under solar irradiation. Most oxides have band gaps wider than the UV energy because of the deeper O 2p potential of the valence band. The valence band of nitrides is composed of the shallower N 2p potential, and thus their band gaps are generally narrower than those of oxides. For photocatalytic water splitting, photoexcited electrons in the conduction band reduce water to evolve hydrogen, and photogenerated holes in the valence band oxidize water to evolve oxygen. Therefore, the potential of the conduction band should be shallower than the reversible hydrogen potential and the potential of the valence band should be deeper than the reversible oxygen potential. In this article, the properties of oxynitride and nitride photocatalysts for water splitting are described.

Surface modification of semiconductor photocatalyst particles with hydrogen- or oxygen-evolving cocatalysts is an indispensable technique in the study of photocatalytic water splitting. In fact, hydrogen-evolution cocatalysts are required

in most cases. A simple illustration of photocatalytic water splitting is shown in Fig. 1. Photoexcited electrons in the conduction band need to be smoothly transferred to the hydrogen-evolution cocatalyst particles without release of energy. The first requirement for the cocatalyst is a smaller barrier for migration of electrons from the semiconductor photocatalyst to the

cocatalyst. The second requirement is that the hydrogen-evolving cocatalysts should have catalytic activity for water reduction. For this, a material with a higher exchange current for water reduction is suitable. A final important requirement is that the cocatalyst should not catalyze the reverse reaction, where the hydrogen produced and oxygen react to form water. Nobel metals, such as

(continued on next page)

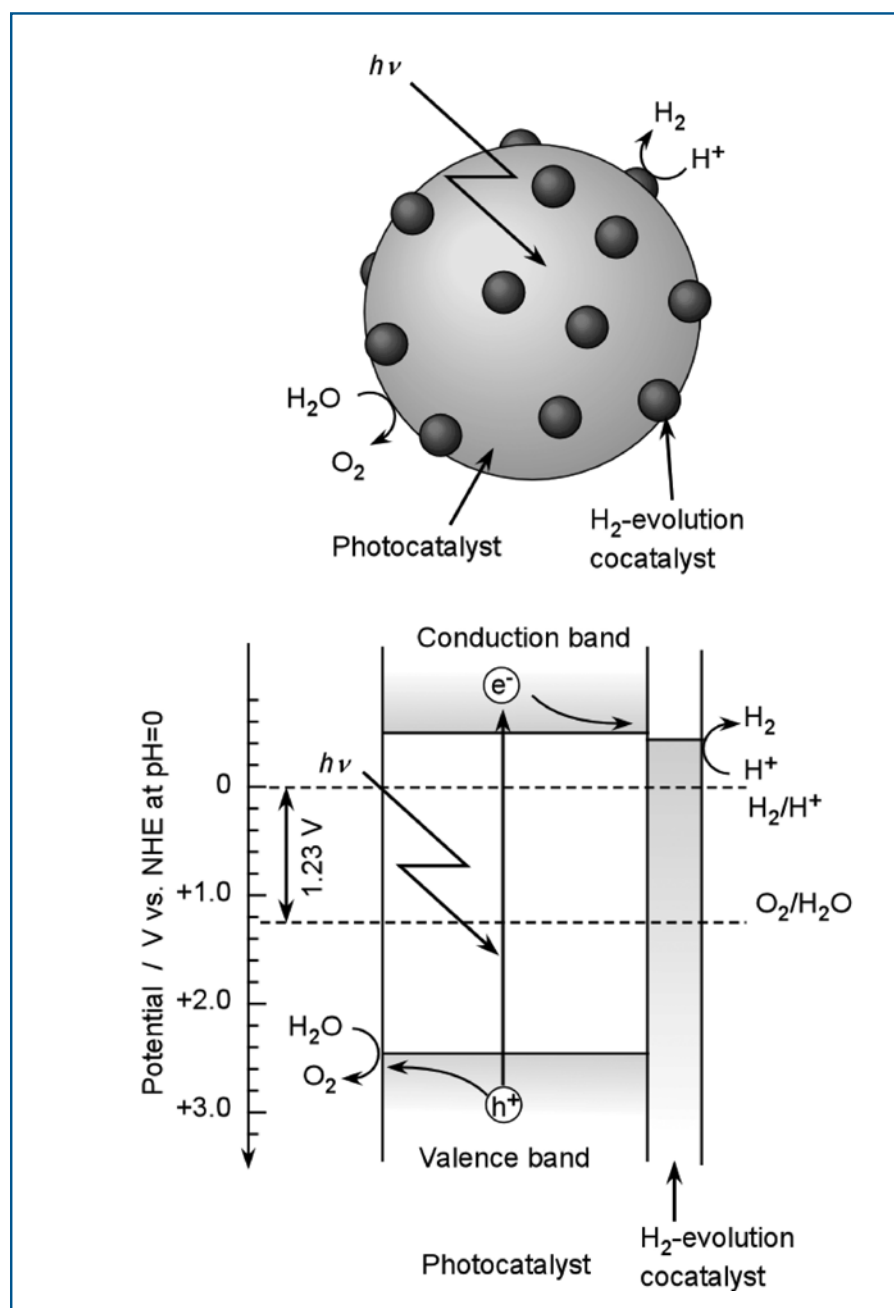


FIG. 1. Schematic illustration and band structure of a photocatalyst for water splitting.

Rh and Pt, are generally active materials for hydrogen evolution; however, they also obviously promote the reverse reaction. Therefore, modification of the cocatalyst surface of Rh with Cr oxide is an effective means of inhibiting the reverse reaction. The development of cocatalysts is key for photocatalytic water splitting.

Photocatalytic Water Splitting with Visible Light

The most active photocatalyst under visible light irradiation is a solid solution of GaN and ZnO, $(\text{Ga}_{1-x}\text{Zn}_x)(\text{N}_{1-x}\text{O}_x)$, modified with a Rh-Cr mixed oxide cocatalyst.⁶⁻⁸ This photocatalyst has an absorption edge at ~ 500 nm and a quantum yield of 5.2 % for 410-nm light, as shown in Fig. 2. The diffuse reflectance spectra of $(\text{Ga}_{1-x}\text{Zn}_x)(\text{N}_{1-x}\text{O}_x)$ is shown in Fig. 3. Although GaN and ZnO are wide gap semiconductors with a wurtzite structure, with absorption edges in shorter wavelength than 400 nm, $(\text{Ga}_{1-x}\text{Zn}_x)(\text{N}_{1-x}\text{O}_x)$ has a longer absorption edge. The reason for the appearance of a new electronic state in the band gap has been explained by theoretical calculations and photoemission spectroscopy.^{9,10}

A glass plate coated with $(\text{Ga}_{1-x}\text{Zn}_x)(\text{N}_{1-x}\text{O}_x)$ photocatalyst can evolve hydrogen and oxygen visually as shown in Fig. 4. The $(\text{Ga}_{1-x}\text{Zn}_x)(\text{N}_{1-x}\text{O}_x)$ photocatalyst was mixed with silica particles and coated on the frosted glass plate. The $(\text{Ga}_{1-x}\text{Zn}_x)(\text{N}_{1-x}\text{O}_x)$ photocatalyst has the highest solar-hydrogen efficiency at present, but the solar-to-hydrogen (STH) conversion efficiency remains at about 0.2% because it mainly utilizes light with a wavelength of 400 nm. The utilization of longer wavelength light in solar irradiation is the key to improving efficiency.

Another promising candidate for photocatalytic water splitting is a mixed oxide with a perovskite structure. NaTaO_3 and SrTiO_3 , which have a perovskite structure, show obvious activity for overall water splitting.^{1,2} In particular, NaTaO_3 doped with La and modified with a NiO cocatalyst has been reported to have a 50% quantum efficiency for 280-nm light.^{3,4} However, these oxide photocatalysts with perovskite structures have an absorption edge in the UV region, and cannot utilize solar irradiation. Our strategy for the development of photocatalysts with the ability to absorb visible light involves the substitution of oxygen with nitrogen. For example, one of the oxygen atoms of SrTiO_3 can be substituted with a nitrogen atom while balancing the charge by replacement of Sr(II) with La(III), yielding LaTiO_2N .^{2,11,12} Because the potential of the 2p orbital of nitrogen is shallower than that of oxygen, the obtained oxynitrides have a narrower band gap than the oxides. Diffuse reflectance spectra of LaTiO_2N and BaTaO_2N are shown

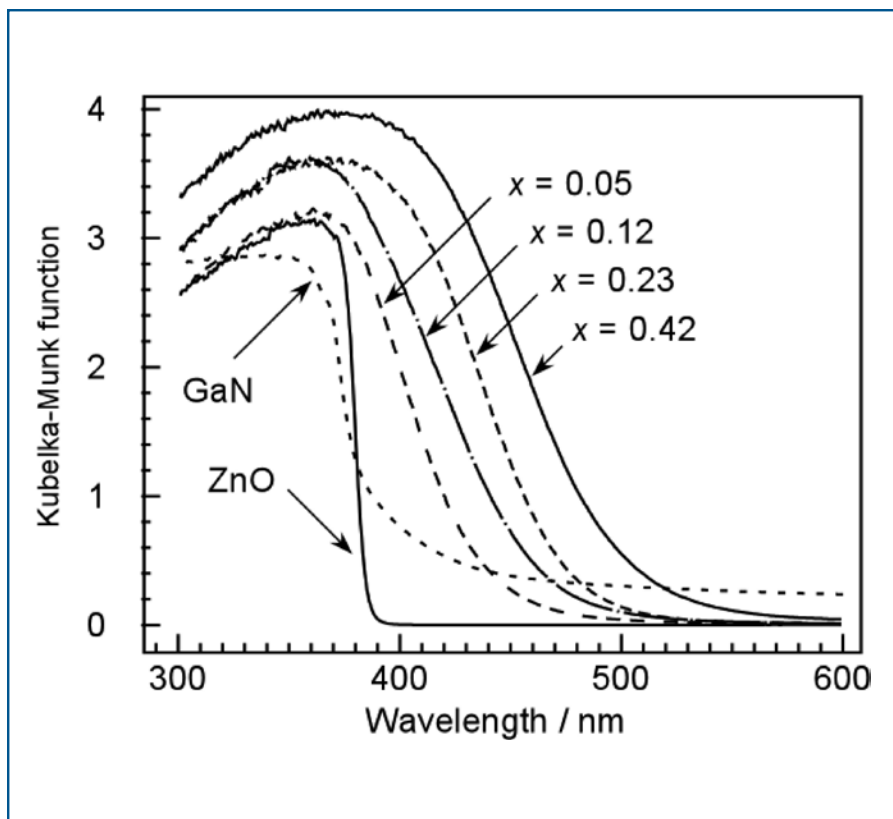


Fig. 2. Diffuse reflection UV-visible spectra of $(\text{Ga}_{1-x}\text{Zn}_x)(\text{N}_{1-x}\text{O}_x)$ with varying x .⁶⁻⁸ GaN and ZnO have absorption edges in the UV region (< 400 nm), but the solid solution has absorption in the visible region.

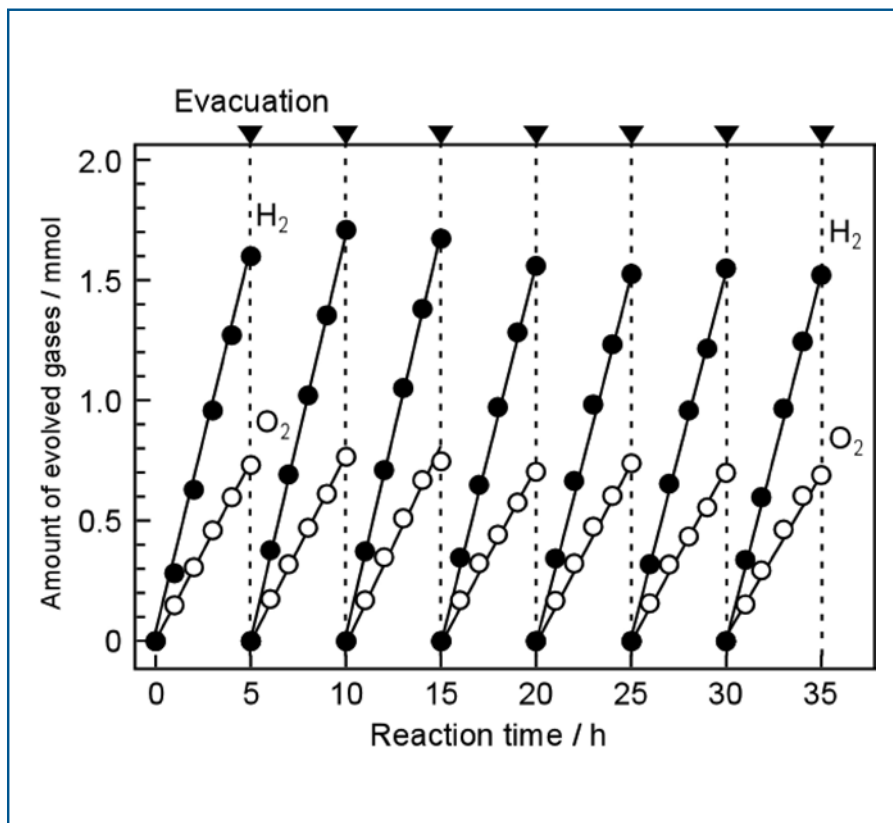


Fig. 3. Gas evolution rates from water for the $(\text{Ga}_{1-x}\text{Zn}_x)(\text{N}_{1-x}\text{O}_x)$ photocatalyst.⁶⁻⁸ 1 wt% Rh and 1.5 wt% Cr were deposited on $(\text{Ga}_{1-x}\text{Zn}_x)(\text{N}_{1-x}\text{O}_x)$. The pH of the water was adjusted to 4.5 by the addition of H_2SO_4 . The light source was a 450-W high-pressure Hg lamp and UV light was absorbed by a NaNO_2 solution as a filter.

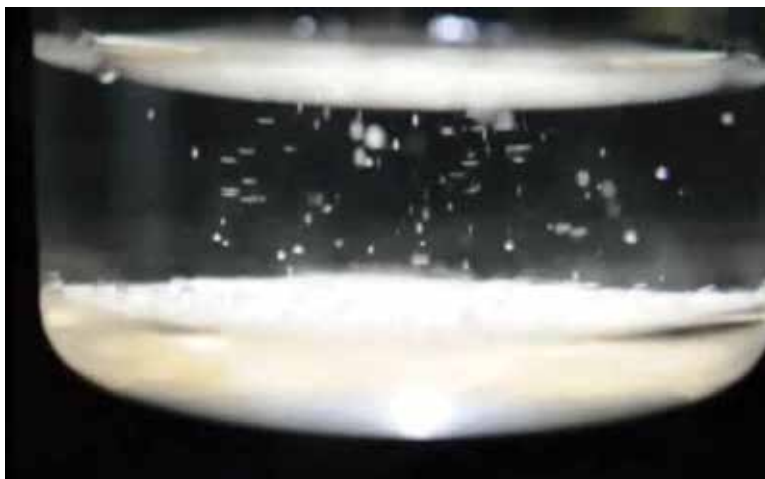


Fig. 4. Photograph of hydrogen and oxygen evolution from $(\text{Ga}_{1-x}\text{Zn}_x)(\text{N}_{1-x}\text{O}_x)$ coated glass plate under irradiation with a 300-W Xe lamp. The surface of the $(\text{Ga}_{1-x}\text{Zn}_x)(\text{N}_{1-x}\text{O}_x)$ was modified with an Rh-Cr mixed oxide. The bubbles consist of a mixture of H_2 and $1/2\text{O}_2$.

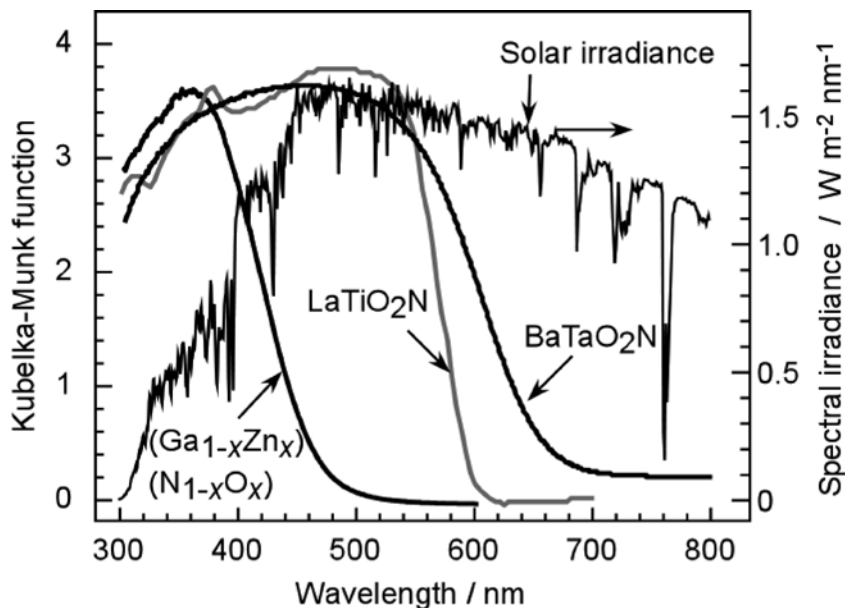


Fig. 5. Diffuse reflection UV-visible spectra of $(\text{Ga}_{1-x}\text{Zn}_x)(\text{N}_{1-x}\text{O}_x)$, LaTiO_2N , and BaTaO_2N .¹¹⁻¹³ Solar irradiance of air mass (AM) of 1.5 G is also shown in the figure.¹⁴ LaTiO_2N and BaTaO_2N utilize more energy of the solar irradiation.

in Fig. 5.¹¹⁻¹³ While $(\text{Ga}_{1-x}\text{Zn}_x)(\text{N}_{1-x}\text{O}_x)$ can absorb 500 nm light, LaTiO_2N and BaTaO_2N can absorb light with a wavelength of 600-700 nm. The solar irradiance is also shown in Fig. 5,¹⁴ and the advantage of LaTiO_2N and BaTaO_2N in the absorption spectra is obvious.

The photoelectrochemical properties of LaTiO_2N thin films are shown in Fig. 6.¹⁵ The LaTiO_2N thin film was epitaxially deposited on Nb:SrTiO_3 substrates by RF magnetron sputtering. A photocurrent appeared below 0 VRHE, indicating that the potential of the conduction band of LaTiO_2N is shallower than the reversible potential for hydrogen evolution. In practical terms, LaTiO_2N and BaTaO_2N can evolve hydrogen and oxygen from sacrificial reagents of methanol and AgNO_3 aqueous solutions, respectively, as shown in Fig. 7.^{11,12} However, overall water splitting by LaTiO_2N or BaTaO_2N has not yet been achieved. We are currently examining tactics for improving the crystallinity, and also surface modification schemes for inhibiting carrier recombination.

Carrier Migration from Photocatalyst to Co-Catalyst

Modification of photocatalysts with co-catalysts is one of the most important issues in the development of photocatalysts. In particular, co-catalysts are required for hydrogen evolution because the conduction band potential is close to the hydrogen evolution potential with an unsatisfactory overpotential. Furthermore, oxide and oxynitride surfaces are not active for the hydrogen evolution reaction. For the $(\text{Ga}_{1-x}\text{Zn}_x)(\text{N}_{1-x}\text{O}_x)$ photocatalyst, a combination of Rh and Cr acts as the hydrogen evolution co-catalyst. When $(\text{Ga}_{1-x}\text{Zn}_x)(\text{N}_{1-x}\text{O}_x)$ is modified with only Rh, the obtained oxygen is reduced on the Rh surface to form H_2O , so that the hydrogen and oxygen evolution rates are dramatically suppressed. However, the addition of Cr inhibits the reduction of oxygen at the Rh surface due to the formation of a Cr layer on the Rh surface as a barrier for oxygen, as shown in Fig. 8.^{16,17} A detailed mechanism has been proposed for this based on the use of model electrodes.^{16,17}

Figure 9 shows infrared spectra of CO adsorbed on a Pt cocatalyst on $(\text{Ga}_{1-x}\text{Zn}_x)(\text{N}_{1-x}\text{O}_x)$ and LaTiO_2N photocatalyst under irradiation and in the dark.^{18,19} For Pt/ $(\text{Ga}_{1-x}\text{Zn}_x)(\text{N}_{1-x}\text{O}_x)$, the absorption peak due to the CO stretching mode was shifted to a lower frequency by the irradiation. It is known that CO adsorbed on electrochemical interfaces shifts the absorption peak due to the changing potential of the electrodes. When the potential shifts to a negative value (shallower), the CO vibration shifts to a lower frequency because of the electrochemical Stark effect or back-donation of electrons of the metal to the $2\pi^*$ orbital of CO. The observed frequency shift can thus be explained by the photoexcited

(continued on next page)

electrons in the photocatalyst particles migrating to the Pt co-catalyst, resulting in a potential shift at the Pt co-catalyst. In the case of the LaTiO_2N photocatalyst, no shift was observed for the CO adsorbed on the Pt co-catalyst, indicating that photoexcited electrons cannot smoothly migrate to most of the Pt particles. We consider that a solution to this undesired phenomenon will open the way to achieving overall water splitting with LaTiO_2N photocatalysts.²⁰ Macroscopic design of photocatalyst particles was also proposed for efficient carrier separation.²¹

Future of Photocatalytic Water Splitting

Figure 10 shows the H_2 evolution rate and STH energy conversion efficiency as a function of the band gap energy of the photocatalysts as single step photocatalysis with a quantum yield of 100%. It is assumed that photons with wavelengths shorter than the value on the horizontal axis are converted to $1/2\text{H}_2$. If the photocatalysts utilize visible light up to 600–700 nm with a quantum yield of 50%, the STH efficiency reaches ~10%, which is equivalent to that of a commercial photovoltaic system. Photocatalytic water splitting devices are obviously simpler than photovoltaic systems because vacuum processing is not required for the preparation of the devices. Considering the terrestrial equatorial area, $27 \text{ TJ km}^{-2} \text{ day}^{-1}$ of solar energy is expected based on an air mass (AM) of 1.5G^{14} and a 7.6 h day^{-1} irradiation. If a 25 km^2 scale solar plant is available and working with 10% STH efficiency, 570 tons day^{-1} of hydrogen can be produced. This is equivalent to the output of typical natural gas plants.

Acknowledgment

This work was supported in part by a Grant-in-Aid for Specially Promoted Research (#23000009) of the Japan Society for the Promotion of Science (JSPS) and the Advanced Low Carbon Technology Research and Development Program (ALCA) of the Japan Science and Technology Agency (JST). This work also contributes to the international exchange program of the A3 Foresight Program of JSPS.

About the Authors

JUN KUBOTA is an Associate Professor in the Department of Chemical System Engineering, the University of Tokyo. He earned a PhD in science from Tokyo Institute of Technology in 1995 and became an Assistant Professor at the Chemical Resources Laboratory, Tokyo Institute of Technology in the same year. He was promoted to an Associate Professor in

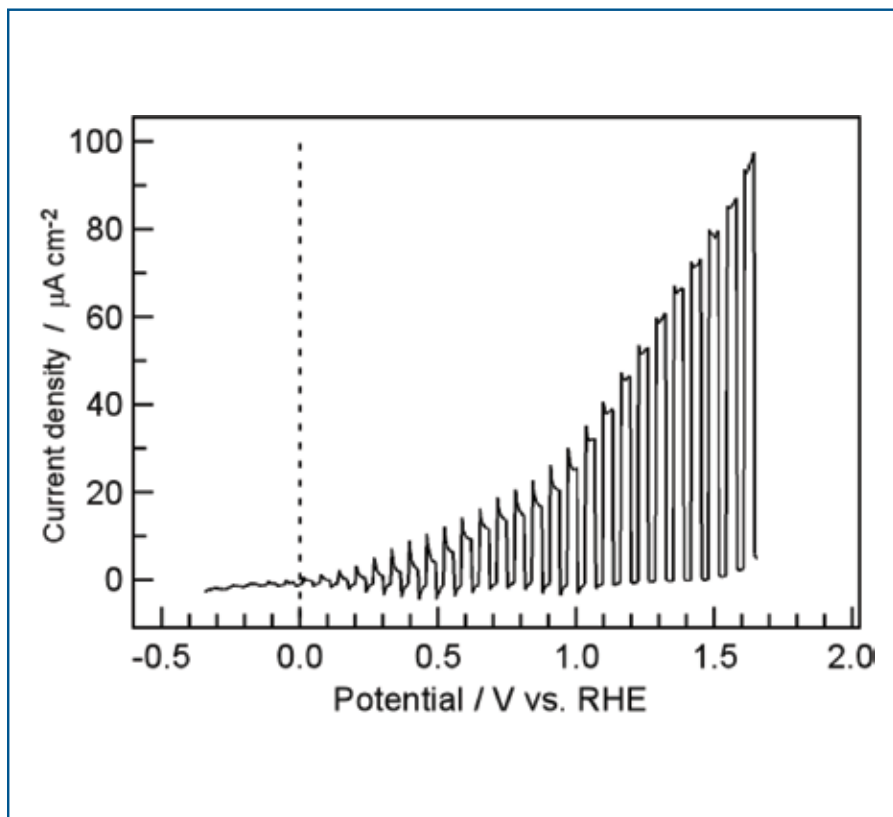


FIG. 6. Current density-potential curve for LaTiO_2N photoelectrode grown epitaxially on a Nb:SrTiO_3 substrate under intermittent irradiation.¹⁵ The photoelectrode surface was modified by IrO_2 nanoparticles as an oxygen evolution cocatalyst. The electrolyte used was $0.5 \text{ M Na}_2\text{SO}_4$, which was adjusted to $\text{pH} = 4.5$ by the addition of H_2SO_4 . An Ag/AgCl reference electrode was used in the experiments and the potential is expressed against a reversible hydrogen electrode (RHE).

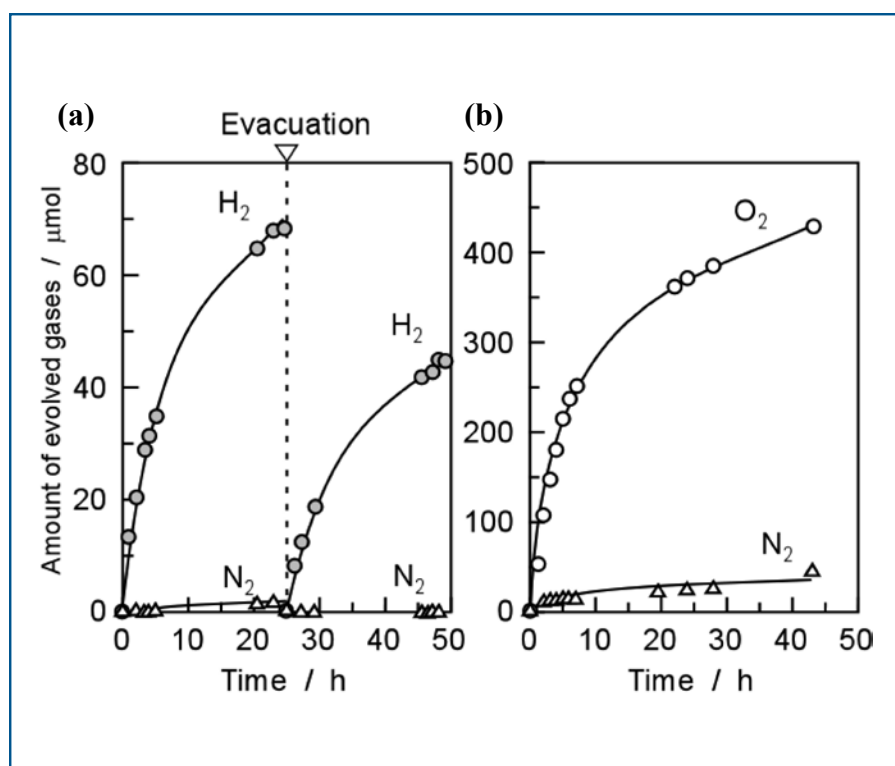


FIG. 7. Hydrogen and oxygen evolution by LaTiO_2N photocatalysts from sacrificial reagents of 20 vol% methanol and 0.01 M AgNO_3 , respectively.^{11,12} For hydrogen evolution, 3 wt% of Pt was loaded on LaTiO_2N by an impregnation method. For oxygen evolution, $0.2 \text{ g of La}_2\text{O}_3$ was added into the reactant to stabilize pH . The light source was a 300-W Xe lamp with a 420-nm cut filter.

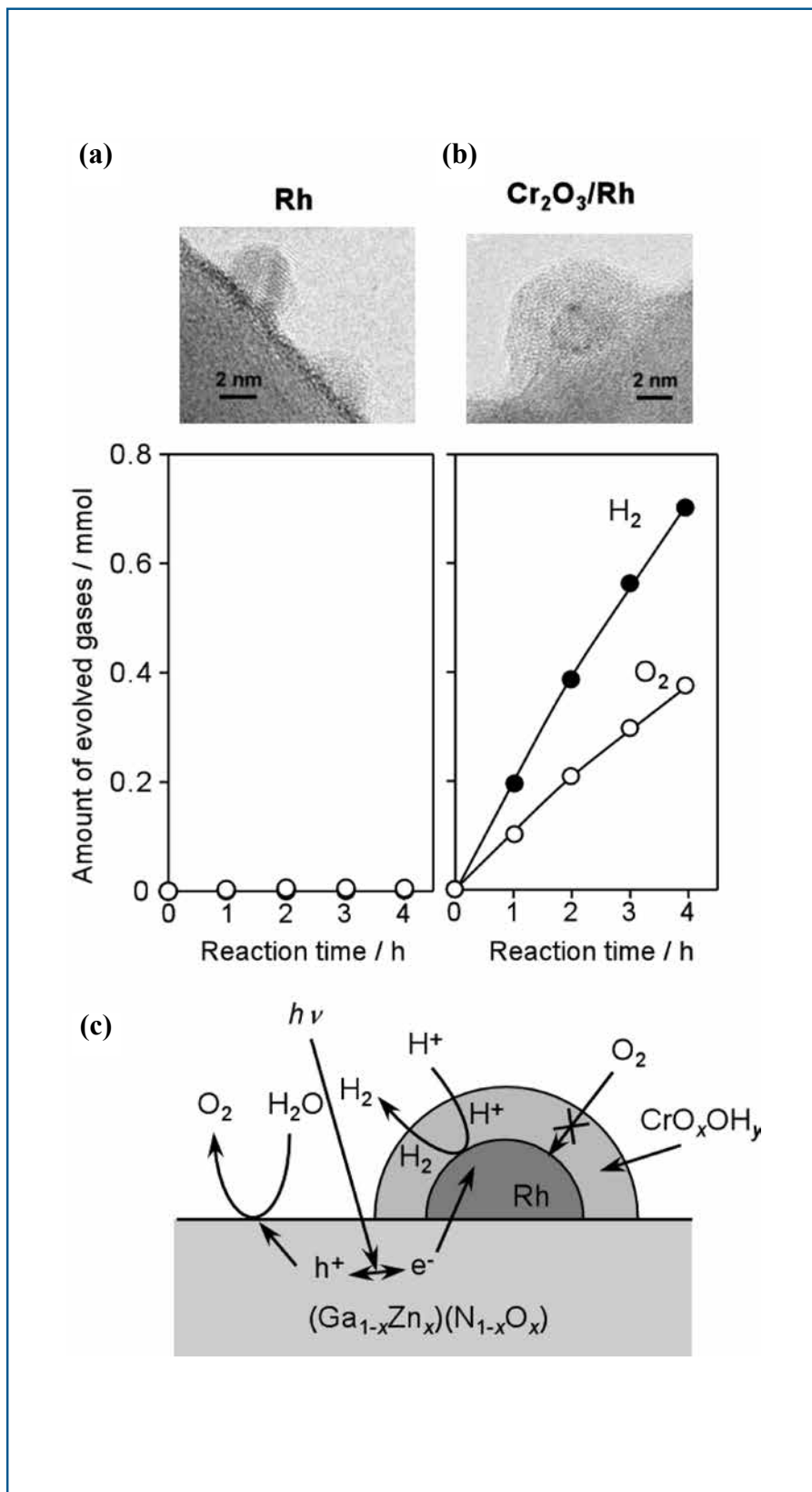


FIG. 8. Transmission electron microscopy images and gas evolution rates of $(\text{Ga}_{1-x}\text{Zn}_x)(\text{N}_{1-x}\text{O}_x)$ photocatalysts with an Rh co-catalyst (a) and a $\text{Cr}_2\text{O}_3/\text{Rh}$ co-catalyst (b). The proposed mechanism of the $\text{Cr}_2\text{O}_3/\text{Rh}$ structure is shown in (c).^{16,17}

the present institute in 2007. His current research programs involve photocatalytic water splitting, catalysts for polymer electrolyte fuel cells (PEFCs), and infrared spectroscopic analysis of solid oxide fuel cells (SOFCs). He may be reached at jkubota@chemsys.t.u-tokyo.ac.jp

KAZUNARI DOMEN is a Professor in the Department of Chemical System Engineering at the University of Tokyo. He became an Assistant Professor at the Chemical Resources Laboratory, Tokyo Institute of Technology in 1982. He was promoted to an Associate Professor in 1990, and then to Full Professor in 1996. He moved to the University of Tokyo in 2004. His current research programs involve photocatalytic water splitting, photoelectrochemical water splitting, and catalysts for polymer electrolyte fuel cells (PEFCs). He received an award from The Chemical Society of Japan in FY2010 for his research in photocatalytic water splitting. Details of his research can be found at <http://www.domen.t.u-tokyo.ac.jp/>. He may be reached at domen@chemsys.t.u-tokyo.ac.jp.

References

1. K. Maeda and K. Domen, *J. Phys. Chem. C*, **111**, 7851 (2007).
2. K. Maeda, T. Takata, and K. Domen, *Energy Efficiency and Renewable Energy Through Nanotechnology*, Ling Zang Ed., Springer, p. 487 (2011).
3. H. Kato and A. Kudo, *Catal. Lett.*, **58**, 153 (1999).
4. H. Kato, K. Asakura, and A. Kudo, *J. Am. Chem. Soc.*, **125**, 3082 (2003).
5. Y. Sakata, Y. Matsuda, T. Yanagida, K. Hirata, H. Imamura, and K. Teramura, *Catal. Lett.*, **125**, 22 (2008).
6. K. Maeda, T. Takata, M. Hara, N. Saito, Y. Inoue, H. Kobayashi, and K. Domen, *J. Am. Chem. Soc.*, **127**, 8286 (2005).
7. K. Maeda, K. Teramura, D. Lu, T. Takata, N. Saito, Y. Inoue, and K. Domen, *Nature*, **440**, 295 (2006).
8. K. Maeda, K. Teramura, and K. Domen, *J. Catal.*, **254**, 198 (2008).
9. M. Yoshida, T. Hirai, K. Maeda, N. Saito, J. Kubota, H. Kobayashi, Y. Inoue, and K. Domen, *J. Phys. Chem. C*, **114**, 15510 (2010).
10. T. Hirai, K. Maeda, M. Yoshida, J. Kubota, S. Ikeda, M. Matsumura, and K. Domen, *J. Phys. Chem. C*, **111**, 18853 (2007).

(continued on next page)

11. A. Kasahara, K. Nukumizu, G. Hitoki, T. Takata, J. N. Kondo, M. Hara, H. Kobayashi, and K. Domen, *J. Phys. Chem. A*, **106**, 6750 (2002).
12. A. Kasahara, K. Nukumizu, T. Takata, J. N. Kondo, M. Hara, H. Kobayashi, and K. Domen, *J. Phys. Chem. B*, **107**, 791 (2003).
13. M. Higashi, R. Abe, K. Teramura, T. Takata, B. Ohtani, and K. Domen, *Chem. Phys. Lett.*, **452** 120 (2008).
14. Electricity, Resources & Building Systems Integration Center, National Renewable Energy Laboratory, U.S. Dept. of Energy (DOE), Solar Resource Data, ASTM G-173 Air Mass 1.5.
15. C. L. P. Thivet, A. Ishikawa, A. Ziani, L. L. Gendre, M. Yoshida, J. Kubota, F. Tessier, and K. Domen, *J. Phys. Chem. C*, **113** 6156 (2009).
16. K. Maeda, K. Teramura, D. Lu, N. Saito, Y. Inoue, and K. Domen, *Angew. Chem. Int. Ed.*, **45**, 7806 (2006).
17. M. Yoshida, K. Takanabe, K. Maeda, A. Ishikawa, J. Kubota, Y. Sakata, Y. Ikezawa, and K. Domen, *J. Phys. Chem. C*, **113**, 10151 (2009).
18. M. Yoshida, A. Yamakata, K. Takanabe, J. Kubota, M. Osawa, and K. Domen, *J. Am. Chem. Soc.*, **131**, 13218 (2009).
19. X. Lu, A. Bandara, M. Katayama, A. Yamakata, J. Kubota, and K. Domen, *J. Phys. Chem. C*, **115**, 23902 (2011).
20. F. Zhang, A. Yamakata, K. Maeda, Y. Moriya, T. Takata, J. Kubota, K. Teshima, S. Oishi, and K. Domen, *J. Am. Chem. Soc.*, **134**, 8348 (2012).
21. T. Hisatomi, T. Minegishi, and K. Domen, *Bull. Chem. Soc. Jpn.*, **85**, 647(2012).

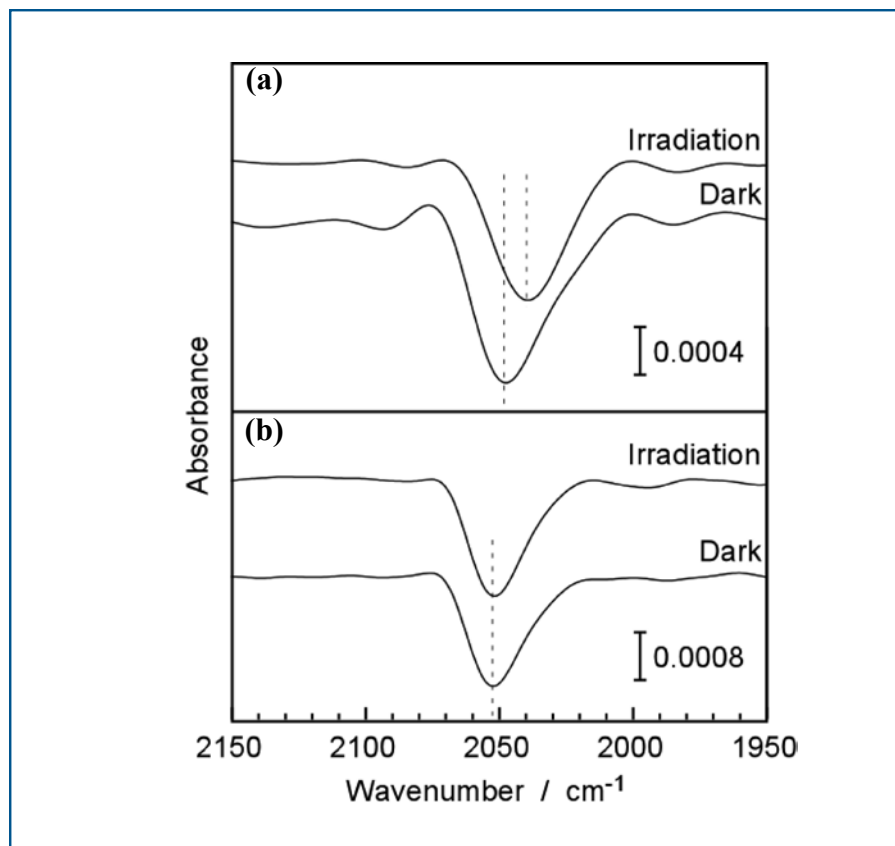


FIG. 9. In situ infrared spectra of CO adsorbed on Pt co-catalysts on $(\text{Ga}_{1-x}\text{Zn}_x)(\text{N}_{1-x}\text{O}_x)$ (a) and $\text{LaTiO}_{2.9}\text{N}$ (b) in Na_2SO_4 aqueous solution before and after irradiation.¹⁹

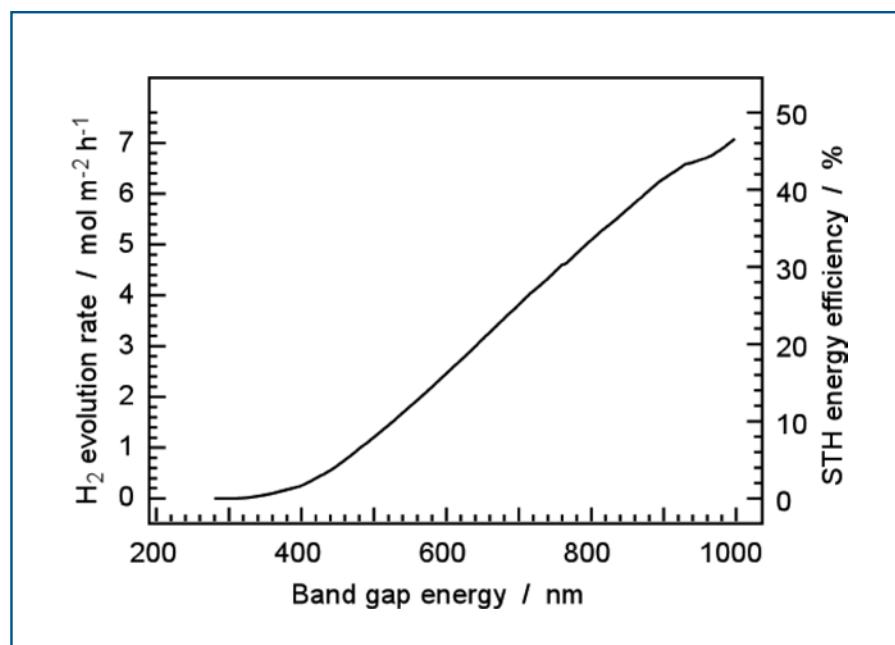


FIG. 10. Theoretical relation of H_2 evolution rate and solar-to-hydrogen conversion efficiency to the band gap energy of photocatalysts in wavelength units. The solar light is assumed to be air mass (AM) 1.5 G^{14} , and 100% quantum yield is assumed.